Water Science & Technology

IWA PUBLISHING

Water Science & Technology Vol 84 No 4, 954 doi: 10.2166/wst.2021.295

Hydraulic performance of helical-step dropshaft

Weichen Ren[a,b], Jianhua Wu[a,*], Fei Ma[a] and Shangtuo Qian[c]

[a] College of Water Conservancy and Hydropower Engineering, Hohai University, Nanjing 210098, China
[b] Department of Hydraulics, State Key Laboratory of Simulation and Regulation of Water Cycle in River Basin, China Institute of Water Resources and Hydropower Research, Beijing 100038, China
[c] College of Agricultural Engineering, Hohai University, Nanjing 210098, China
*Corresponding author. E-mail: jhwu@hhu.edu.cn

JW, 0000-0003-1346-9046

ABSTRACT

Aiming to achieve energy dissipation and prevention of cavitation erosion, a kind of dropshaft in urban drainage systems called the helical-step dropshaft is introduced in this paper. It dissipates flow energy by means of step geometry and prevents cavitation erosion through air entrainment. To verify its availability, the hydraulic characteristics of the helical-step dropshaft were experimentally investigated, including the flow regimes, the efficiency of energy dissipation, characteristics of air entrainment and pressure distribution. The results demonstrate that, even for a large discharge, flow can be discharged smoothly and steadily, and a high energy-dissipation rate of over 87% is achieved. There are three distinct flow regimes observed in the dropshaft, namely nappe flow, mixed flow and skimming flow. Moreover, there is no less than 1.6% air concentration and a reasonable pressure distribution on the step surface. This study provides an attractive alternative for the design of drop structures.

Key words: air entrainment, drop structure, energy dissipation, helical-step dropshaft, urban drainage system

HIGHLIGHTS

- A novel helical-step dropshaft prototype was modelled and verified by experimentally studying its hydraulic characteristics.
- Flow regimes in the dropshaft were specially observed and a novel mixed flow regime for the helical stepped chute was defined and described.
- Air concentration near the step surface was measured to help understand the cavitation prevention in the helical-step dropshaft for the first time.

NOTATION

b	step height;
c	helical stepped chute width;
D	dropshaft diameter;
d_a	air vent pipe diameter;
E_1, E_2	energy head of calculated sections 1 and 2;
g	gravity acceleration;
H	dropshaft height;
H_1	vertical drop height of per turn;
h_1, h_2	flow depth of calculated sections 1 and 2;
Q	model discharge;
v_1, v_2	mean velocity of calculated sections 1 and 2;
Z_1, Z_2	elevation of calculated section 1 and 2;
α_1, α_2	energy correction coefficient;
β	central angle of each step;
η	energy dissipation ratio.

INTRODUCTION

Global climate change and rapid urbanization have led to more extreme rainfall events and thus the increasing risks of urban flooding disasters in China (Hallegatte *et al.* 2013; Zhang *et al.* 2016). As an effective strategy for coping with this problem, urban deep tunnel drainage systems have been constructed for decades in many countries, such as the USA, Canada and Japan (Guo & Song 1990; Toda & Inoue 1999). Now those kinds of projects are being planned in China.

As a key element in urban deep-tunnel drainage systems, dropshafts are used to convey water from a high elevation to an underground deep tunnel. During water transportation, almost the same volume of air in the tunnel needs to be released from the tunnel. With the development of urban constructions, dropshafts in urban drainage systems are characterized prominently by large discharges and large drop heights. For example, recent projects planned in Shanghai and Wuhan require some dropshafts with drop heights of up to 40–80 m and discharges of over 45 m^3/s. Large drop heights and discharges can generate a large amount of energy and high risk of cavitation erosion. Experience drawn from the Donghaoyong Deep-Tunnel Drainage System in Guangzhou, the only deep tunnel in operation in China, as well as previous projects, demonstrates that energy dissipation and prevention of cavitation erosion have become two major challenges for the design of dropshaft structures (Rajaratnam *et al.* 1997; Ma *et al.* 2007; He *et al.* 2017).

In past decades, four main types of dropshafts have been used, divided into two categories. The first category includes the early plunge type and vortex type. The plunge dropshaft, which directs water to freely fall in a vertical shaft, is the oldest and simplest type (Rajaratnam *et al.* 1997; Chanson 2002). Its geometry could be square, rectangular or circular (Chanson 2004; Granata *et al.* 2011). It should be noted that tall plunge dropshafts can entrain a significant amount of air into the tunnel, in some cases reaching over a hundred times the water flow rate (Zhang *et al.* 2015), which may cause air pressurization in the downstream tunnel and possible dangerous geysering problems (Guo & Song 1990; Edwini-Bonsu & Steffler 2006). As a result, many recent studies on plunge dropshafts focus on reducing air entrainment; for example, by additional air vent shafts (Granata *et al.* 2014; Ma *et al.* 2017; Wei *et al.* 2018). Vortex dropshafts let the flow spiral down the vertical shaft, essentially clinging along the shaft walls, and the air moves as a central air core (Jain 1987; Fernandes & Jónatas 2019). Proper inflow preconditioning is crucial for the dropshaft, and there are several standard inlet configurations used to produce vortex flow and maintain a stable air core, such as circular, scroll, spiral and tangential, with their design guidelines detailed in previous work (Jain & Kennedy 1983; Hager 1990; Yu & Lee 2009). The other category includes two improved dropshafts, which contain independent air vent pipes, namely, helicoidal ramp dropshafts and baffle dropshafts. The helicoidal ramp dropshaft is designed on the basis of the traditional vortex-type dropshaft. An additional smooth helical ramp is added to increase the friction loss between the flow and the helical ramp, and to obviate the deaeration chamber at the bottom of the dropshaft (Kennedy *et al.* 1988). This structure is popular in Japan but is not extensively preferred elsewhere. A modern baffle-type dropshaft was also discussed (Odgaard *et al.* 2013; Yang & Yang 2020), and adopted in the Donghaoyong Deep-Tunnel Drainage System with a maximum prototype discharge of 32 m^3/s. It provides high efficiency of energy dissipation, but the required diameter is much larger than that of other dropshafts (Wang *et al.* 2015; Wei *et al.* 2018).

Due to their simple structure, high energy dissipation and lower cavitation damage risks, stepped spillways have been widely used in hydropower projects, and their hydraulic characteristics have been systematically investigated (e.g., by Chanson (1995), Matos (2000), Boes & Hager (2003a), Ohtsu *et al.* 2004). Accordingly, a kind of dropshaft called the helical-step dropshaft was developed, which has the advantages of stepped energy dissipaters (Wu & Ren 2016; Ren *et al.* 2019), and now this design is adopted in Shanghai deep-tunnel drainage system. Despite some favor by engineers, few achievements about the hydraulic characteristics about the helical-step dropshaft were reported. Similar dropshafts with large-angle steps or blade-shaped steps were tested by means of experimental and numerical methods, respectively, and these case studies provided some useful information about the flow characteristics in the dropshafts (Qi *et al.* 2018; Wu *et al.* 2018; Sun *et al.* 2020). Attention was also paid to the standing waves formed at the inlet of such dropshafts in the literature (Wu *et al.* 2017). However, the performance and mechanism of the energy dissipation and cavitation erosion reduction in the dropshaft are yet to be investigated to support the design. Hence, it is of great importance to comprehensively explore the hydraulics of the helical-step dropshaft.

To evaluate the performances of energy dissipation and air entrainment of the helical-step dropshaft and validate the design, a helical-step dropshaft was physically modelled and its hydraulic characteristics were experimentally tested, including the flow regimes, energy dissipation and characteristics of air entrainment and pressure distribution.

Helical-step dropshaft

The helical-step dropshaft described herein, as shown in Figure 1, consists of an air vent pipe at its center and a continuous helical stepped chute attached to the wall. The air vent pipe allows for air movement between the dropshaft and the atmosphere, and also helps mitigate surge. Unlike vortex-type dropshafts, helical-step dropshafts do not require specially designed inlet geometry to precondition the flow. Flow is directed into the dropshaft and is discharged along the helical stepped chute and then leaves the dropshaft tangentially. In this process, the flow energy is dissipated by means of the step geometry. For small discharges, the energy is mainly dissipated by a series of jet breaks in the air, jet impact and mixing on the steps, and the formation of a fully or partially developed hydraulic jump. For large discharges, most of the energy is dissipated by vortices between the steps and by intensive turbulence. Meanwhile, air entrainment is enhanced, and thus a properly aerated flow is formed to protect the step structures from cavitation damage. Through these mechanisms, energy dissipation and reduction in cavitation damage are satisfied in the helical-step dropshaft.

EXPERIMENTAL SETUP AND METHODOLGY

Experimental setup

The experiments were conducted in the High-Speed Flow Laboratory of Hohai University in Nanjing, China. The experimental setup consisted of a pump, a flow meter, a large feeding basin, a test model and a flow return system. The test model, as illustrated in Figure 2, made of Perspex for visual observation, includes a rectangular approach flow channel, a dropshaft and

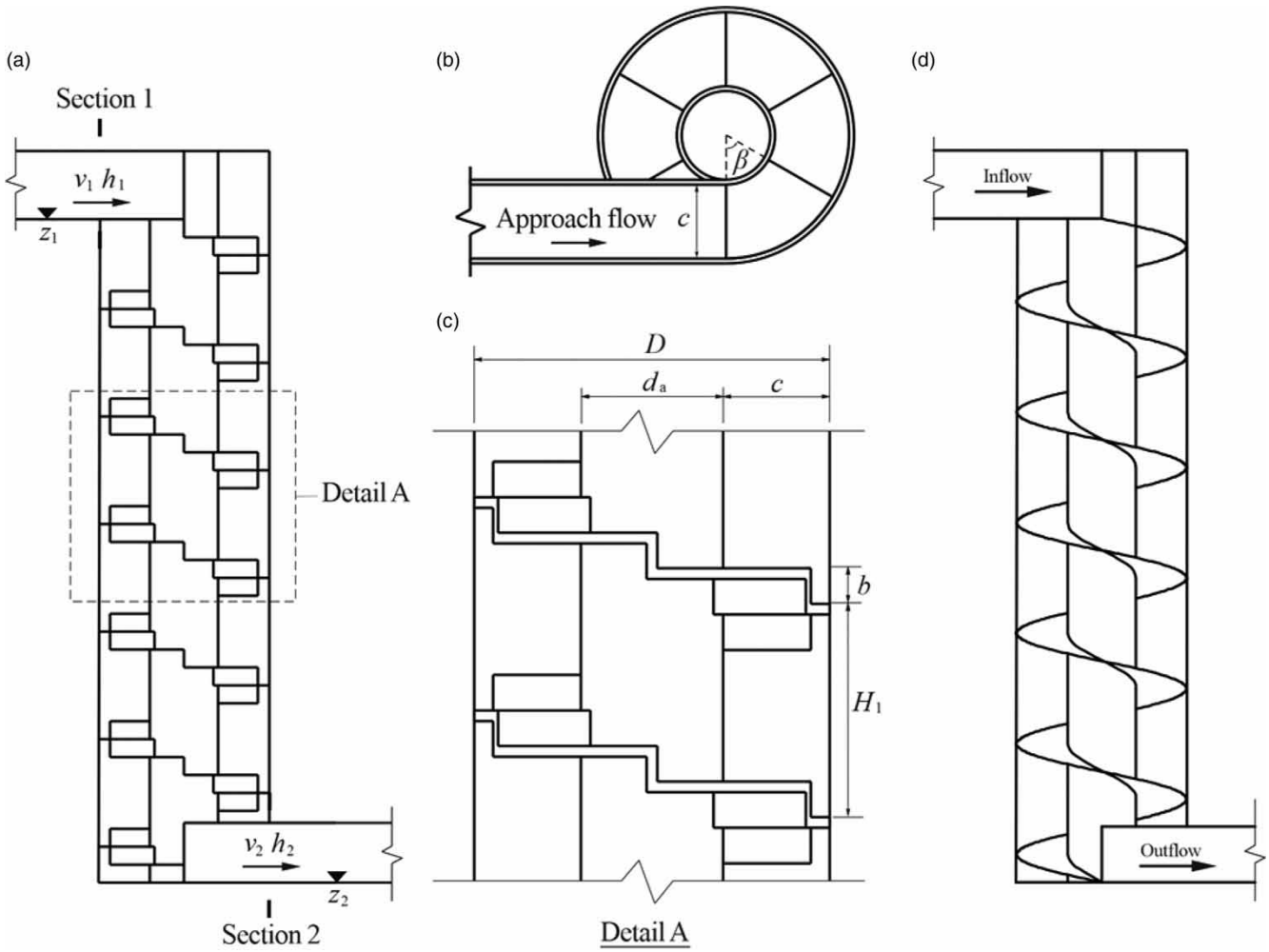

Figure 1 | Schematic of dropshafts: (a) main view, (b) top view, (c) detail view for the helical-step dropshaft, and (d) the helicoidal ramp dropshaft.

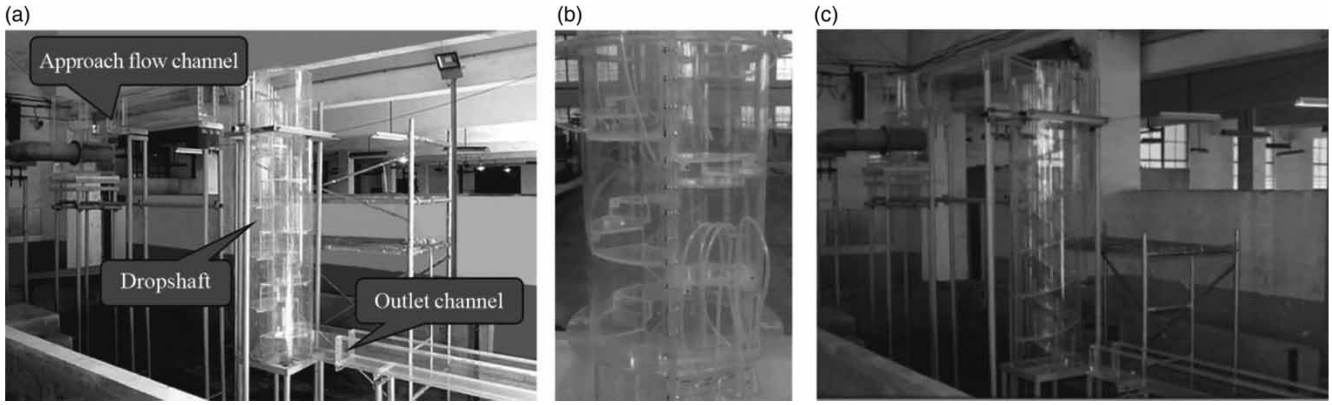

Figure 2 | Photographs: (a) side view of the test model, (b) detail view of the helical-step dropshaft, (c) side view of the helicoidal ramp dropshaft.

an outlet channel. The helical-step dropshaft model replicated a future prototype serving the city of Shanghai, with a geometrical scale factor of 1:20. As scaled, the model might be sufficiently large to limit scale effects.

The approach flow channel was 2.50 m long and 0.15 m wide, and there was an intake box upstream in the channel where rectifying measures were taken to help stabilize the flow. Thus a steady approach flow condition was obtained in the channel. The helical-step dropshaft diameter was $D = 0.50$ m, the diameter of the air vent pipe at the center was $d_a = 0.20$ m, and the width of the helical stepped chute in the dropshaft was $c = 0.15$ m. The helical stepped chute consisted of 36 steps with 6 turns; that is, each step corresponded to a central angle $\beta = 60°$, and the step height was $b = 0.055$ m. Thus, the vertical drop per turn was $H_1 = 6b = 0.33$ m, and the total drop of the dropshaft was $H = 6H_1 = 1.98$ m. The flat bottom outlet channel, 0.15 m wide and 6.00 m long, was connected with the dropshaft model for the observation and measurement of outflow conditions.

In this experiment, a helicoidal ramp dropshaft was also made for comparison. The schematic diagram and photo are shown in Figures 1(d) and 2(c), respectively. It consisted of a vertical circular shaft with a continuous helicoidal ramp attached to the shaft wall and an air vent hole, and its configuration was similar to that of the helical-step dropshaft model, including the same $D = 0.50$ m, $d_a = 0.20$ m, $H_1 = 0.33$ m, and $H = 1.98$ m. The helicoidal-ramp dropshaft model shared the same inflow and outflow conditions with the helical-step dropshaft model.

Experimental methodology

The hydraulic characteristics of the helical-step dropshaft were investigated under different working conditions; that is, discharge Q. And it is useful to express the flow discharge in terms of a dimensionless flow discharge Q^* defined by $Q^* = Q/(gR^5)^{0.5}$, where the acceleration of gravity $g = 9.81$ m/s^2, R = radius of the dropshaft. There were 5 working conditions to make the measurement in the experiment: $Q = 5.0$, 10.0, 15.0, 20.0 and 25.0 l/s, corresponding to $Q^* = 0.051$, 0.102, 0.153, 0.204, 0.255. The discharge rate was measured by a Metran MTF-S200-7AP electromagnetic discharge meter (made by Metlan Measuring and Controlling Instrument Co., Ltd, China) installed in the flow return system, with a relative accuracy of $\pm 0.2\%$.

The energy dissipation of the dropshaft η can be defined as $\eta = (E_1 - E_2)/E_1$, where $E_1 = h_1 + Z_1 + \alpha_1 v_1^2/(2g)$ and $E_2 = h_2 + Z_2 + \alpha_2 v_2^2/(2g)$ are the total heads of the calculated sections 1 and 2, respectively [see Figure 1(a)]. Here, h_1 and h_2 are the flow depths (m) at sections 1 and 2 respectively (measured by a Vernier depth gauge), Z_1 and Z_2 are the elevations (m), v_1 and v_2 are the corresponding mean velocities (m/s) calculated by dividing the discharge by the flow area, and the kinetic energy correction coefficients $\alpha_1 = \alpha_2 = 1.0$ approximately. Specific measurement results of the flow depth h_2 were obtained 2.00 m downstream of section 2, where the flow was steadier and air entrained by the dropshaft had almost detrained, resulting essentially in black water flow, and the head difference from section 2 can be neglected. There was uncertainty in the determination of flow depth because of flow turbulence and surface fluctuations. Flow depths in channels had estimated maximum errors 2 mm in the inlet and about up to 4 mm in the more fluctuant flow in the outlet. As a compromise, at least five times repeated measurements on flow depth were made in the experiment to minimize the random error, and the average were taken as the final results. Considering the error propagation, the maximum relative error of the flow head is estimated to be in the order of 6% in the present work.

In the experiment, all 36 steps were numbered downstream from the first step as S1 – S36. Preparatory experiments demonstrated that, except for the first few steps, the flow performances on all the steps were similar. Therefore, the two steps, S19 and S36 in the middle and the end of the dropshaft, respectively, were chosen as representatives to study the air entrainment and time-averaged pressure distribution.

Four time-averaged pressure gauging points were evenly distributed on the bottom of each step along the flow direction. For air concentration gauging points on each step, there were four points on the bottom, and four on the outer sidewall, 0.03 m from the bottom, with uniform distribution along the flow direction. The plane positions of all the gauging points are shown in Figure 3.

The time-averaged pressure was measured using a piezometer and the air concentration was recorded using a CQ6-2005 aeration apparatus (made by China Institute of Water Resources and Hydropower Research). Its sampling rate and period are 1020 Hz and 20 s, respectively, and the accuracy is $\pm 0.3\%$. More information about this probe can be found in Qian *et al.* (2016).

RESULTS AND DISCUSSION

Flow observation

Flow performances in the helical-step dropshaft were observed in this experiment. The flow entered the dropshaft almost tangentially and then went down along the helical stepped chute. In general, water was discharged smoothly and steadily through the helical-step dropshaft because it experienced no abrupt changes in direction or speed (see Figure 4). Significantly, the desirable flow behaviour was maintained even when the dimensionless discharge was $Q^* = 0.272$ in the present experiment.

It is generally acknowledged that there are distinct flow regimes defined for the standard stepped spillway; that is, nappe flow and skimming flow, separated by a transition regime. Extensive research has been developed to describe and distinguish these flow regimes (e.g. Boes & Hager 2003a, 2003b; Chanson & Toombes 2004; Bung 2013). One of the most noticeable differences is the flow behavior in step corners. Nappe flow and skimming flow may be distinguished roughly by the presence of air cavities or flow recirculation in step corners. For the helical-step dropshaft, specific observation was made on the flow behavior in step corners, and flow regimes are discussed and defined accordingly.

With increasing discharges, specifically, three different flow behaviors occurred on the steps in the dropshaft, namely nappe flow, mixed flow and skimming flow, as depicted in Figure 5. Their difference might be easily noticed by observing the behavior of the air cavity in the step corner, as shown in Figure 6.

For small discharge $Q^* \leq 0.069$, a free-falling nappe is found on each step surface (see nappe flow in Figure 5(a)), and an air cavity is maintained in the step corner, which refers to Figure 6(a) in which a clear air-water interface could be found. For large discharge $Q^* > 0.077$ in Figure 5(c), skimming flow is observed. Stable recirculating vortices develop between the steps and the water flows as a coherent stream. The step corner was fully filled with water, as shown in Figure 6(c). These

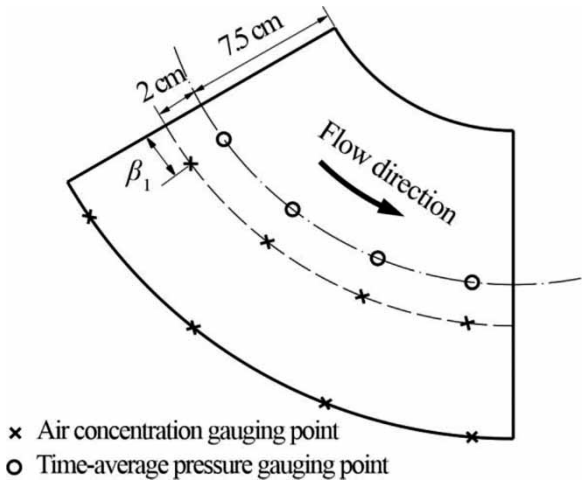

Figure 3 | Plane position of all the gauging points on S36.

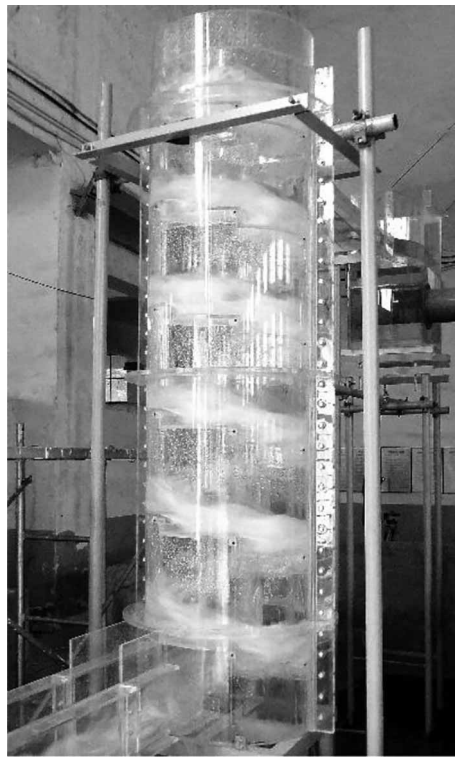

Figure 4 | General view of flow performance in the dropshaft.

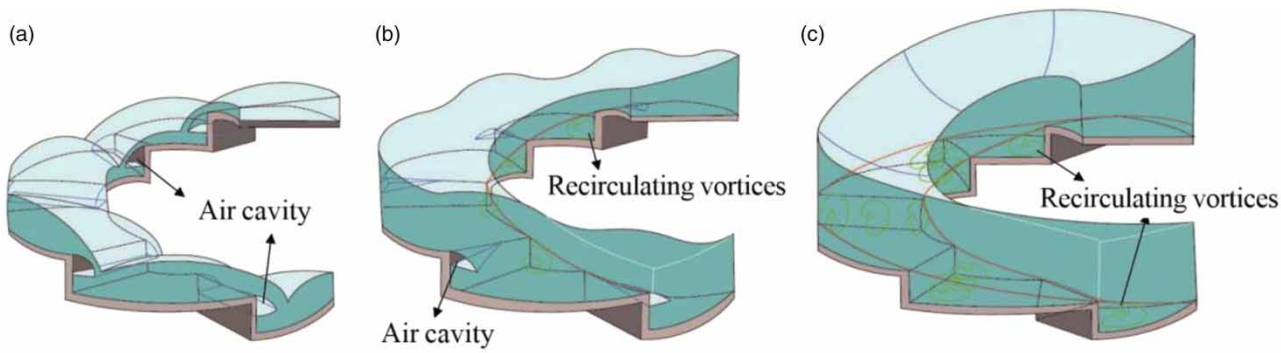

Figure 5 | Flow regimes in the helical-step dropshaft: (a) nappe flow, (b) mixed flow and (c) skimming flow.

two flow regimes are similar to those on standard stepped spillways. Numerical simulation made by Sun *et al.* (2020) verified these two flow regimes in the dropshaft, with no other flow patterns reported and classified.

It is found that, however, a mixed flow regime existed between these two regimes (within a relatively small range of $0.069 < Q^* \leq 0.077$) in the present work. The mixed flow behavior could be seen on each step (see Figure 5(b)). In the width direction, the air cavity on the inner side was filled with water vortices that supported a coherent stream, while the flow on the outer side was still characterized by the free-falling jet. Figure 4(b) shows a clear air cavity on the outer side, and the air-water interface disappears in the middle of the step. The flow features were neither those of nappe flow nor skimming flow. The flow did not exhibit the quasi-homogeneous appearance observed in skimming flow and on each step, obvious variations of flow properties were observed in the width direction. It is believed that such a three dimensional flow behavior may refer to a new flow regime that is associated with the special geometrical conditions of the helical stepped chute.

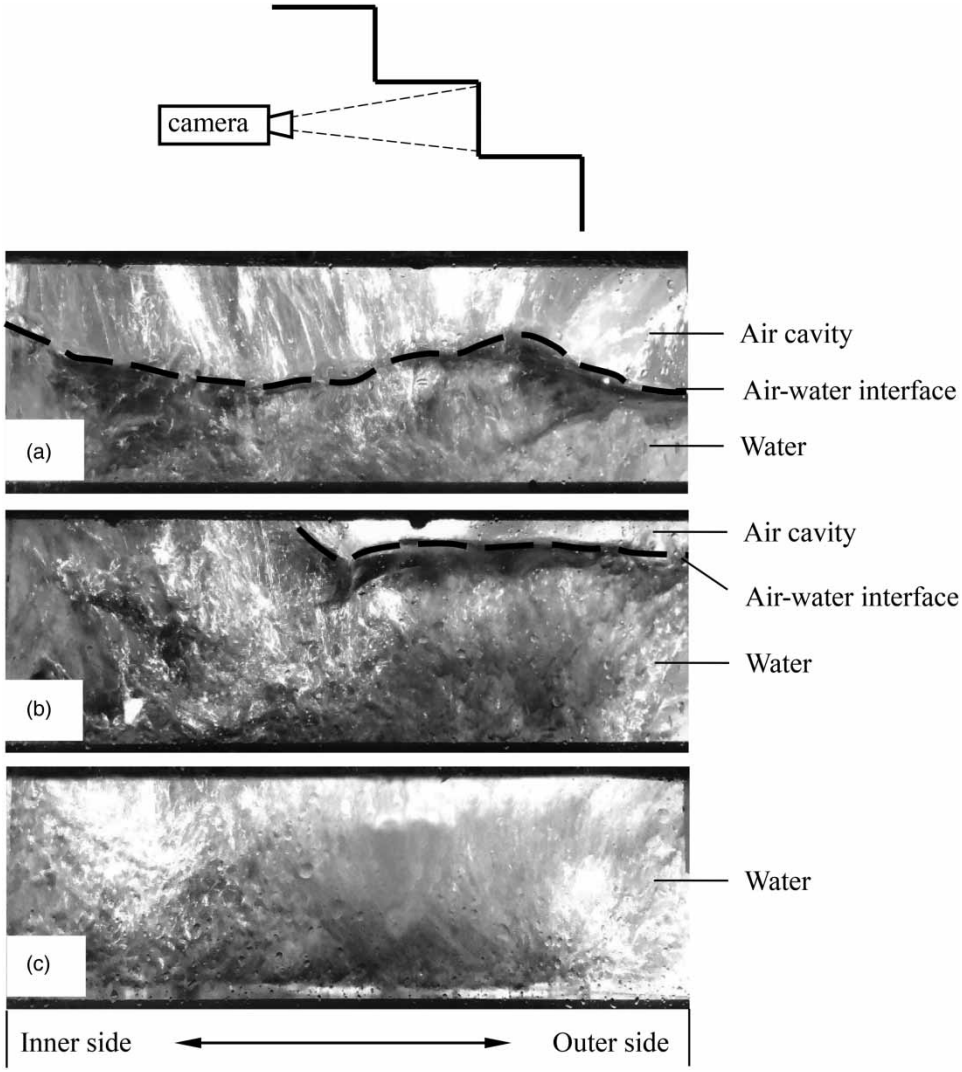

Figure 6 | Observations of air pocket behavior (view underneath the helical stepped chute): (a) nappe flow, (b) mixed flow and (c) skimming flow.

The mixed flow behavior could be understood in that the chute slope varies in the width direction because of the special design of the helical stepped chute in the dropshaft. The inner side of the helical stepped chute is steeper than the outer side, and air cavities on this side are more easily filled with water with the increasing flow discharges. Under a certain range of discharge, the mixed flow regime occurs.

This mixed regime is completely different from the transition flow regime on the standard stepped spillway. The transition flow is defined as both nappe and skimming flow behaviors occurring simultaneously on different steps, as well as strong splashing, which is highlighted by significant flow variations on different steps and some instabilities for one discharge (Ohtsu & Yasuda 1997; Chanson & Toombes 2004). For the mixed regime described herein, mixed behavior could be observed on each step, and it is also quite stable. It should be noted that the flow observation in the present experiment is primitive, and detailed flow regime classification on the helical stepped chute might have to be further investigated with different step geometries.

Energy dissipation

Figure 7 demonstrates how the energy dissipation η varies with Q^* and changes in kinetic and potential energy between the entrance and the outlet of the helical-step dropshaft and helicoidal ramp dropshaft. The relative energy losses of these two

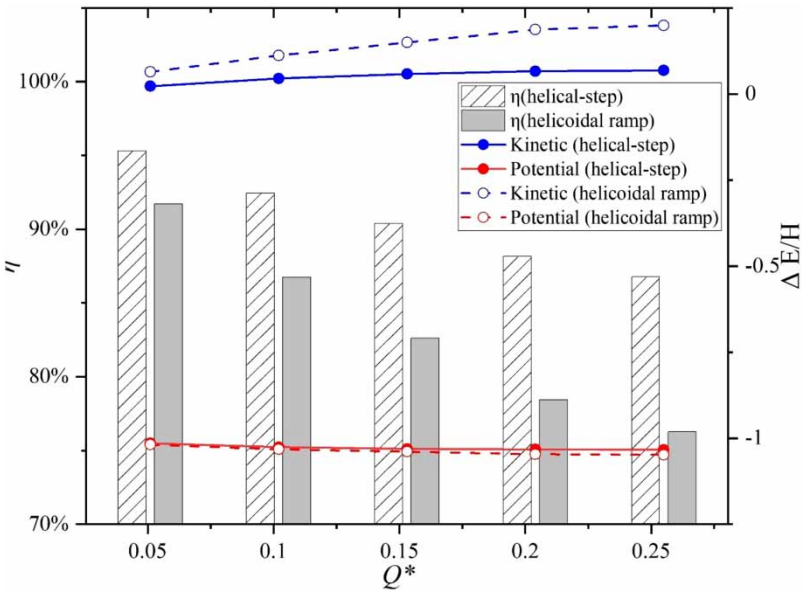

Figure 7 | Variation of η and changes in dimensionless kinetic and potential energy, with Q^*.

kinds of dropshafts decrease with the increasing discharge rates. This trend is consistent with the numerical results by Sun *et al.* (2020). However, the helical-step dropshaft had around 95% ~ 87% energy dissipation during the experiments. In comparison, the energy dissipation of the helicoidal ramp dropshaft (91% ~ 76%) is noticeably less than that of the helical-step dropshaft, and this difference becomes more significant for larger discharge rates. Changes in the kinetic energy and potential energy between the entrance and the outlet of the two dropshafts are in accord with the aforementioned characteristics. The value of changes in the kinetic energy are considerably smaller than that of potential energy, suggesting that only a small part of the potential energy was converted to the kinetic energy and most of the potential energy were consumed in the dropshafts. And it is found that for the helicoidal ramp dropshaft, the increment in kinetic energy is obviously larger than that of the helical-step dropshaft, which means larger kinetic energy at the outlet of the helicoidal ramp dropshaft given the same inflow condition. In practice, additional dissipative measures (e.g., water cushion) may be necessary to protect the structures downstream the helicoidal ramp dropshaft.

It should be noted that for helicoidal ramp dropshafts, energy dissipation occurs as distributed friction loss along the smooth helical channels (Kennedy *et al.* 1988), whereas for helical-step dropshafts, the energy exchange and dissipation process is far more complicated. The dissipative phenomena in a helical-step dropshaft include (a) nappe jet breakup in the air, jet impact and jet mixing on the step; (b) formation and maintain stable vortices in step corners; (c) flow aeration; (d) friction between water and shaft wall and (e) possible hydraulic jump on the step. These phenomena greatly promote the energy consumption of the water. As a consequence, the energy loss carried by the helical-step dropshaft is significantly greater than that of the helicoidal ramp dropshaft. In addition, the high efficiency of the distributed energy dissipation characteristics for the proposed helical-step dropshaft obviates the need for a water cushion at the bottom of the dropshaft. The hydraulic jump in the water cushion is likely to give rise to downstream flow instability (Zhao *et al.* 2006). And it is believed that the geyser phenomenon is associated with such instability in the junction region between inflow structures and tunnels in urban deep-tunnel drainage systems (Cong *et al.* 2017).

Air entrainment

In addition to energy dissipation performance, cavitation erosion might be another serious concern in the design of the drop structure due to the large discharges and drop heights. It is generally agreed that air entrainment could reduce or even, in some cases, avoid cavitation damage. The investigations made by Peterka (1953) describe that when the air concentration is equal to or larger than 1–2% in the model test, cavitation damage can be greatly reduced. In this way, the experimental research about air concentration in the helical-step dropshaft is indispensable.

Table 1 lists the air concentration values obtained from the bottom and sidewall of the helical stepped chute at steps S19 and S36, where β_1 is the position of a gauging point from the step starting point, and β_1/β represents the relative position of the gauging points along the flow direction (see Figure 3).

As seen in Table 1, first, air concentration measurements on steps S19 and S36 are generally similar. In addition to almost the same flow performance on the vast majority of steps, it is suggested that a steady air entrainment along the helical stepped chute and the measurement results on steps S19 and S36 could represent the basic characteristic of the air concentration distribution along the helical stepped chute. Second, the air concentrations on the bottom and sidewall of the step decrease as the discharge rates increase. These observations are consistent with the test results for standard stepped spillways (Zhang *et al.* 2012; Xu *et al.* 2015). It is noteworthy that for the small discharges $Q^* = 0.051$ and 0.102, air concentrations in the middle region of the step are larger than those on both sides of the step, as the middle region is just where the plunging jet impacts into the recirculating pool. In this region, not only is some air entrained by the plunging jet action but also a significant volume of spray is generated by the impact on the step, which also contributes to the air entrainment (Toombes *et al.* 2008). It is believed that the mechanism of air entrainment in the dropshaft is in line with that on stepped chutes because of flow similarity. Flows are characterized by the high level of turbulence, and air bubble entrainment is caused by turbulence fluctuations acting next to the free surface. Furthermore, although the air concentration decreases with increasing discharges, the air concentration at the bottom and sidewall turns out to be 1.6% for $Q^* = 0.255$ in this experiment, which might be sufficient to greatly reduce or even avoid cavitation damage in the dropshaft.

Time-average pressure distribution

The time-averaged pressure measurements were obtained for the steps in the helical-step dropshaft and the normalized pressure heads ($P/\rho gb$, where ρ is the water density) are shown in Figure 8.

It can be seen from Figure 8 that the time-averaged pressure distribution on the different steps is generally similar. The average pressure on the step surface increases with the increasing discharge, and at the same time, the distribution characteristics vary significantly, which can be roughly divided into two situations. In the case of small discharges, such as $Q^* = 0.051$ and 0.102, the pressure on the step surface presents a uniform distribution, and the values are approximately equal to the water depth on the step. This is in accord with observations in standard stepped spillways, as for small discharges, step bottoms are often characterized by hydrostatic behaviour (Sánchez-Juny & Dolz 2005). This is because there is a limited amount of water falling from the higher step and a small amount of energy is carried by the falling jet. Thus, the jet can have little effect on the water cushion on the step bottom. It is also worth noting that the pressure distribution shows a downward trend in the region near the step edge. This may be attributed to the effect of the falling jet formed here. For large discharges, the pressure distribution on the step surface changes drastically. With the increase of the flow discharges, there is a slight increment in the pressure in the upstream half region. This part of the area is mainly dominated by the recirculating vortices. In contrast, a pressure boost on the middle-downstream parts of the step bottom is measured as a result of the enhanced jet impingement effect.

The maximum pressure appears in the region around $\beta_1/\beta = 0.6$. Therefore, more attention should be paid to this region when considering the strength of the step structures.

Table 1 | Air concentration for the bottom and sidewall of the helical stepped chute (%)

		Q^*				
Number	β_1/β	**0.051**	**0.102**	**0.153**	**0.204**	**0.255**
S19	0.10	3.1/[a]	2.7/3.1	2.4/2.5	2.3/2.4	2.2/2.2
	0.37	4.6/3.0	3.7/2.5	3.4/2.2	2.6/2.2	2.1/2.1
	0.63	3.3/2.8	2.8/2.8	2.4/2.5	2.0/2.3	1.8/2.1
	0.90	3.0/2.8	2.4/2.8	2.0/2.2	1.8/2.3	1.6/2.0
S36	0.10	3.7/[a]	2.5/3.8	2.7/2.9	2.5/2.5	2.1/2.2
	0.37	5.2/3.2	4.6/2.8	3.9/2.6	3.8/2.5	2.3/2.1
	0.63	4.4/2.6	3.8/2.3	2.7/2.2	2.2/2.3	2.0/2.2
	0.90	3.1/2.4	2.8/2.1	2.1/2.2	1.9/2.4	1.8/2.0

Note: In the term '*x*/*y*' of the air concentration data, *x* and *y* are experimental data on the bottom and the outer sidewall, respectively.
[a]Measurement is invalid due to the air-exposed point that occurs when the discharge is small.

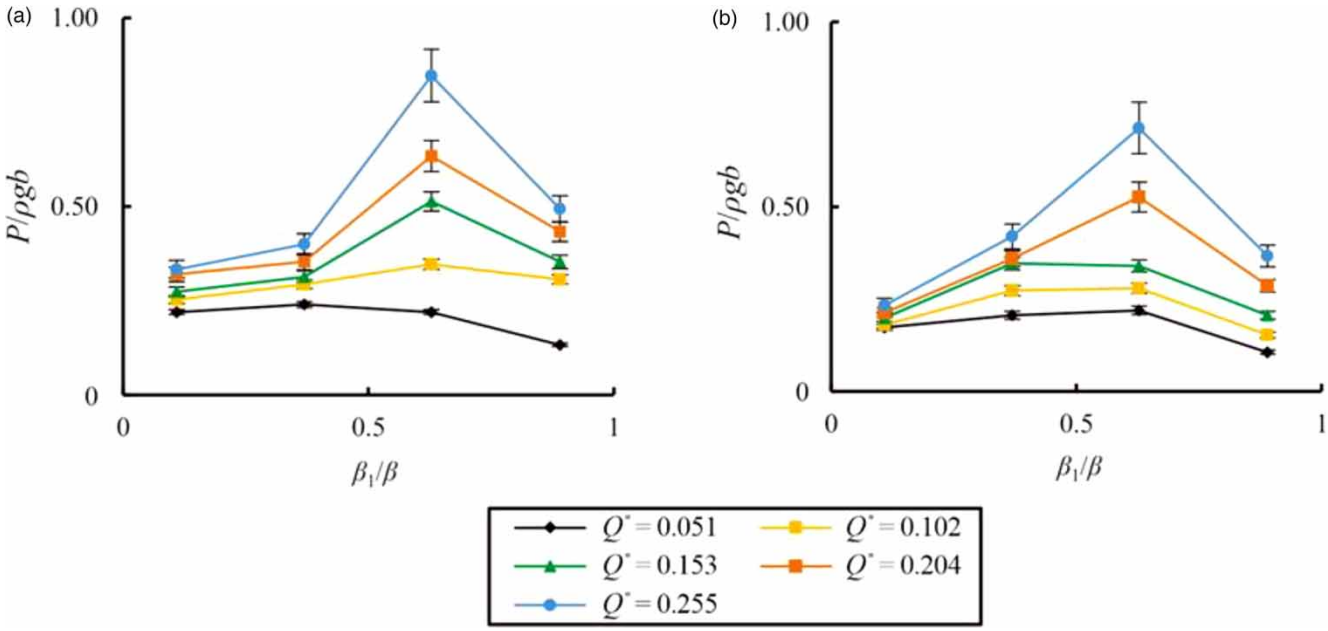

Figure 8 | Pressure measurements for bottom of steps: (a) S19; (b) S36.

CONCLUSIONS

A kind of dropshaft, called the helical-step dropshaft, was introduced in this paper, which aims to achieve energy dissipation and prevent cavitation erosion. The practicability of this design was demonstrated by the desirable flow behaviour, high efficiency of energy dissipation, proper air entrainment and pressure distribution during the flow discharging. The main findings are as follows.

First, water can be conveyed by the helical-step dropshaft smoothly and steadily, with the discharge up to $Q^* = 0.272$ in this experiment. Second, a novel mixed flow, as well as nappe flow and skimming flow, could be defined as three kinds of distinct flow regimes in the dropshaft. Third, the energy dissipation of the helical-step dropshaft decreases with increasing discharges, but still maintains 87% for the maximum discharge in the experiment, which is obviously better than that of the helicoidal ramp dropshaft. Fourth, the air concentration at the bottom and sidewall of the step decreases as the discharge increases. No less than 1.6% air concentration is measured, which might indicate an acceptable efficiency of preventing cavitation erosion. Additionally, there is a reasonable pressure distribution observed. Moreover, because of similar flow performance, it is believed some achievements of standard stepped spillways may also be applicable for this helical-step dropshaft.

The present design provides an attractive alternative for drop structures in urban deep-tunnel drainage systems, especially for large drop heights and large discharges. Obviously, there are still some issues awaiting further investigation: (a) characteristics of the mixed flow regime, (b) energy dissipation evaluation with different geometric conditions considered and (c) maximum discharge capability and design guidelines.

ACKNOWLEDGEMENTS

This work is funded by the National Natural Science Foundation of China under grant (No. 51779081 and 51979082); the Fundamental Research Funds for the Central Universities under grant (No. 2017B622X14) and the Postgraduate Research & Practice Innovation Program of Jiangsu Province under grant (No. KYCX17_0433). The first author acknowledges the financial support from the National Key Research and Development Program of China (Grant No. 2016YFC0401706) and IWHR Research & Development Support Program (No. HY0145B422016). Ms Fan Tang is gratefully acknowledged for the assistance in the production of Figure 5.

DATA AVAILABILITY STATEMENT

All relevant data are included in the paper or its Supplementary Information.

REFERENCES

Boes, R. M. & Hager, W. H. 2003a Hydraulic design of stepped spillways. *Journal of Hydraulic Engineering* **129** (9), 671–679. doi: 10.1061/(ASCE)0733-9429(2003)129:9(671).

Boes, R. M. & Hager, W. H. 2003b Two-phase flow characteristics of stepped spillway. *Journal of Hydraulic Engineering* **129** (9), 661–670. doi: 10.1061/(ASCE)0733-9429(2003)129:9(661).

Bung, D. B. 2013 Non-intrusive detection of air-water surface roughness in self-aerated chute flows. *Journal of Hydraulic Research* **51** (3), 322–329. doi: 10.1080/00221686.2013.777373.

Chanson, H. 1995 *Hydraulic Design of Stepped Cascades, Channels, Weirs and Spillways*. Pergamon, Oxford, UK.

Chanson, H. 2002 An experimental study of Roman dropshaft hydraulics. *Journal of Hydraulic Research* **40** (1), 3–12. doi: 10.1080/00221680209499868.

Chanson, H. 2004 Hydraulics of rectangular dropshafts. *Journal of Hydraulic Engineering* **130** (6), 523–529. doi: 10.1061/(ASCE)0733-9437(2004)130:6(523).

Chanson, H. & Toombes, L. 2004 Hydraulics of stepped chutes: the transition flow. *Journal of Hydraulic Research* **42** (1), 43–54. doi: 10.1080/00221686.2007.9521754.

Cong, J., Chan, S. N. & Lee, J. H. W. 2017 Geyser formation by release of entrapped air from horizontal pipe into vertical shaft. *Journal Hydraulic Engineering.* **143** (9), 04017039. doi: 10.1061/(ASCE)HY.1943-7900.0001332.

Edwini-Bonsu, S. & Steffler, P. M. 2006 Modeling ventilation phenomenon in sanitary sewer systems: a system theoretic approach. *Journal of Hydraulic Engineering* **132** (8), 778–790. doi: 10.1061/(ASCE)0733-9429(2006)132:8(778).

Fernandes, J. & Jónatas, R. 2019 Experimental flow characterization in a spiral vortex drop shaft. *Water Science & Technology* **80** (2), 274–281. doi: 10.2166/wst.2019.274.

Granata, F., Marinis, G. D., Gargano, R. & Hager, W. H. 2011 Hydraulics of circular drop manholes. *Journal of Irrigation and Drainage Engineering* **137** (2), 102–111. doi: 10.1061/(ASCE)IR.1943-4774.0000279.

Granata, F., Marinis, G. D. & Gargano, R. 2014 Air-water flows in circular drop manholes. *Urban Water Journal* **12** (6), 477–487. doi: 10.1080/1573062X.2014.881893.

Guo, Q. & Song, C. C. S. 1990 Surging in urban storm drainage systems. *Journal Hydraulic Engineering* **116** (12), 1523–1537. doi: 10.1061/(ASCE)0733-9429(1990)116:12(1523).

Hager, W. H. 1990 Vortex drop inlet for supercritical approaching flow. *Journal of Hydraulic Engineering* **116** (8), 1048–1054. doi: 10.1061/(ASCE)0733-9429(1990)116:8(1048).

Hallegatte, S., Green, C., Nicholls, R. J. & Corfeemorlot, J. 2013 Future flood losses in major coastal cities. *Nature Climate Change* **3** (9), 802–806. doi: 10.1038/NCLIMATE1979.

He, Z., Wang, B., Yang, Y., Pan, W. & Qu, H. 2017 Review on vertical shaft in urban wastewater drainage system. *China Water and Wastewater* **33** (10), 49–53. doi: 10.19853/j.zgjsps.1000-4602.2017.10.011 (in Chinese).

Jain, S. C. 1987 Free-surface swirling flows in vertical dropshaft. *Journal of Hydraulic Engineering* **113** (10), 1277–1289. doi: 10.1061/(ASCE)0733-9429(1987)113:10(1277).

Jain, S. C. & Kennedy, J. F. 1983 *Vortex-Flow Drop Structures for the Milwaukee Metropolitan Sewerage District Inline Storage System. Rep. No. 264*. Iowa Institute of Hydraulic Research, Iowa City, IA.

Kennedy, J. F., Jain, S. C. & Quinones, R. R. 1988 Helicoidal-ramp dropshaft. *Journal of Hydraulic Engineering* **114** (3), 315–325. doi: 10.1061/(ASCE)0733-9429(1988)114:3(315).

Ma, Y., Zhu, D. Z., Rajaratnam, N. & Duin, B. 2007 Energy dissipation in circular drop manholes. *Journal of Irrigation and Drainage Engineering* **143** (12), 04017047. doi: 10.1061/(ASCE)IR.1943-4774.0001241.

Ma, Y., Zhu, D. Z., Yu, T. & Liu, Y. 2017 Assessing the effectiveness of an airshaft for dropshaft air re-circulation and depressurization. *Journal of Hydro-Environment Research* **18**, 49–62. doi: 10.1016/j.jher.2017.11.001.

Matos, J. 2000 Hydraulic design of stepped spillways over RCC dams. In: *Proceedings of International Workshop on Hydraulics of Stepped Spillway*, Zurich, Switzerland.

Odgaard, A. J., Lyons, T. C. & Craig, A. J. 2013 Baffle drop structure design relationships. *Journal of Hydraulic Engineering* **139** (9), 995–1002. doi: 10.1061/(ASCE)HY.1943-7900.0000761.

Ohtsu, I. & Yasuda, Y. 1997 Characteristics of flow conditions on stepped channels. In: *Proceedings of the 27th IAHR Biennial Congress*, New York, USA.

Ohtsu, I., Yasuda, Y. & Takahashi, M. 2004 Flow characteristics of skimming flows in stepped channels. *Journal of Hydraulic Engineering* **130** (9), 860–869. doi: 10.1061/(ASCE)0733-9429(2004)130:9(860).

Peterka, A. J. 1953 The effect of entrained air on cavatation pitting. In: *Proceedings of Minnesota International Hydraulics Convention*, Minneapolis, Minnesota, US.

Qi, Y., Wang, Y. & Zhang, J. 2018 Three-dimensional turbulence numerical simulation of flow in a stepped dropshaft. *Water* **11** (1), 1–30. doi: 10.3390/w11010030.

Qian, S., Wu, J. & Ma, F. 2016 Hydraulic performance of ski-jump-step energy dissipater. *Journal of Hydraulic Engineering* **142** (10), 05016004. doi: 10.1061/(ASCE)HY.1943-7900.0001178.

Rajaratnam, N., Mainali, A. & Hsung, C. Y. 1997 Observations on flow in vertical dropshafts in urban drainage systems. *Journal of Environmental Engineering* **123** (5), 486–491. doi: 10.1061/(ASCE)0733-9372(1997)123:5(486).

Ren, W., Wu, J. & Ma, F. 2019 Experimental investigation of helical-step dropshaft hydraulics. In: *Proceedings of the 38th IAHR World Congress*, Panama City, Panama.

Sánchez-Juny, M. & Dolz, J. 2005 Experimental study of transition and skimming flows on stepped spillways in RCC dams: qualitative analysis and pressure measurements. *Journal of Hydraulic Research* **43** (5), 540–548. doi: 10.1080/00221680509500152.

Sun, J., Qian, S., Xu, H., Wang, X. & Feng, J. 2020 Three-dimensional numerical simulation of stepped dropshaft with different step shapes. *Water Science & Technology Water Supply* **21**, 1. doi: 10.2166/ws.2020.336.

Toda, K. & Inoue, K. 1999 Hydraulic design of intake structures of deeply located underground tunnel systems. *Water Science and Technology* **39** (9), 137–144. doi: 10.1016/S0273-1223(99)00226-7.

Toombes, L., Wagner, C. & Chanson, H. 2008 Flow patterns in nappe flow regime down low gradient stepped chutes. *Journal of Hydraulic Research* **46** (1), 4–14. doi: 10.1080/00221686.2008.9521838.

Wang, B., Deng, J. Q., He, Z. J. & Wang, J. P. 2015 A study on design constraints for baffle-drop shaft structure. *Journal of China Institute of Water Resource and Hydropower Research* **13** (5), 363–367. doi: 10.13244/j.cnki.jiwhr.2015.05.008 (in Chinese).

Wei, J., Ma, Y., Zhu, D. Z. & Zhang, J. 2018 Experimental study of plunging-flow dropshafts with an internal divider for air circulation. *Journal of Hydraulic Engineering* **144** (9), 06018011. doi: 10.1061/(ASCE)HY.1943-7900.0001510.

Wu, J. & Ren, W. 2016 *Helical-step dropshaft*. Chinese Patent, No. 201620104789.X (in Chinese).

Wu, J., Ren, W. & Ma, F. 2017 Standing wave at dropshaft inlets. *Journal of Hydrodynamics* **29** (3), 524–527. doi: 10.1016/S1001-6058(16)60765-5.

Wu, J., Yang, T., Sheng, J., Ren, W. & Ma, F. 2018 Hydraulic characteristics of stepped spillway dropshafts with large angle. *Chinese Journal of Hydrodynamics* **33** (2), 176–180. doi: 10.16076/j.cnki.cjhd.2018.02.005 (in Chinese).

Xu, W., Luo, S. & Zheng, Q. 2015 Experimental study on pressure and aeration characteristics in stepped chute flows. *Science China Technological Science* **58** (4), 720–726. doi: 10.1007/s11431-015-5783-6.

Yang, Q. & Yang, Q. 2020 Experimental investigation of hydraulic characteristics and energy dissipation in a baffle-drop shaft. *Water Science & Technology* **82** (8), 1603–1613. doi: 10.2166/wst.2020.441.

Yu, D. & Lee, J. H. W. 2009 Hydraulics of tangential vortex intake for urban drainage. *Journal of Hydraulic Engineering* **135** (3), 164–174. doi: 10.1061/(ASCE)0733-9429(2009)135:3(164).

Zhang, J., Chen, J. & Wang, Y. 2012 Experimental study on time-averaged pressures in stepped spillway. *Journal of Hydraulic Research* **50** (2), 236–240. doi: 10.1080/00221686.2012.666879.

Zhang, W., Zhu, D. Z. & Rajaratnam, N. 2015 Use of air circulation pipes in deep dropshafts for reducing air induction into sanitary sewers. *Journal of Environmental Engineering* **142** (4), 04015092. doi: 10.1061/(ASCE)EE.1943-7870.0001046.

Zhang, J., Wang, Y., He, R., Hu, Q. & Song, X. 2016 Discussion on the urban flood and waterlogging and causes analysis in China. *Advances in Water Science* **27** (4), 485–491. doi: 10.14042/j.cnki.32.1309.2016.04.001 (in Chinese).

Zhao, C. H., Zhu, D. Z., Sun, S. K. & Liu, Z. P. 2006 Experimental study of flow in a vortex drop shaft. *Journal of Hydraulic Engineering* **132** (1), 61–68. doi: 10.1061/(ASCE)0733-9429(2006)132:1(61).

First received 27 January 2021; accepted in revised form 13 July 2021. Available online 22 July 2021